Ship resistance when operating in floating ice floes: derivation, validation, and application of an empirical equation

Luofeng Huang[a, *], Zhiyuan Li[b, *], Christopher Ryan[a], Jonas W. Ringsberg[b], Blanca Pena[a], Minghao Li[b], Li Ding[b] and Giles Thomas[a]

[a]Department of Mechanical Engineering, University College London (UCL), London, United Kingdom

[b]Department of Mechanics and Maritime Sciences, Chalmers University of Technology, Gothenburg, Sweden

Abstract: With the effects of global warming, the Arctic is presenting a new environment where numerous ice floes are floating on the open sea surface. Whilst this has improved Arctic shipping navigability in an unprecedented way, the interaction of such floes with ships is yet to be understood to aid the designing of ships and route planning for this region. To further explore this topic, the present work develops a procedure to derive an empirical equation that can predict the effects of such floes on ship resistance. Based on a validated computational approach, extensive data are extracted from simulations of three different ships with varying environmental conditions. The ice-floe resistance is shown to strongly correlate with ship beam, ship buttock angle, ship waterline angle, ship speed, ice concentration, ice thickness and floe diameter, and the regression powers of each of the parameters on resistance are ascertained. This leads to a generic empirical equation that can swiftly predict ice-floe resistance for a given ship in a given condition. Subsequently, demonstrations are given on the incorporation of the derived equation into a set of real-time Arctic ship performance model and voyage planning tool, which can predict a ship's fuel consumption in ice-infested seas and dynamically suggest a route with the least safety concern and fuel consumption. Moreover, the equation is validated by providing ice resistance prediction for experimental and full-scale conditions from multiple sources, showing high accuracy. In conclusion, the empirical equation is shown to give valid and rapid estimates for ice-floe resistance, providing valuable insights into ship designs for the region, as well as facilitating practical applications for polar navigation.

Keywords: Arctic shipping, ice floe, ship resistance, empirical equation, derivation, validation.

*Corresponding authors: ucemlhu@ucl.ac.uk (L. Huang), zhiyuan.li@chalmers.se (Z. Li)

Nomenclature

α	Waterline angle
γ	Buttock angle
ρ_{ice}	Ice density
A	Ice resistance coefficient
B	Ship beam at waterline
C	Ice concentration
D	Equivalent ice diameter of upper surface
Fr	Froude number
g	Gravitational acceleration
h	Ice thickness
L_{pp}	Ship length between perpendiculars
R_{ice}	Ship resistance induced by ice
R_{water}	Ship resistance induced by water
U	Ship speed
AIV	Arctic In-service Vessel
ASPM	Arctic Ship Performance Model
CFD	Computational Fluid Dynamics
DEM	Discrete Element Method
FSICR	Finnish Swedish Ice Class Rules
ITTC	International Towing Tank Conference
JBC	Japan Bulk Carrier
KCS	KRISO Container Ship
NSR	Northern Sea Route
NWP	Northwest Passage
RPM	Revolutions Per Minute
VPT	Voyage Planning Tool

1. Introduction

Climate change has caused Arctic sea ice to melt dramatically, in turn causing an extensive transition from level-ice coverage to broken ice-floe fields and open water [1]. The changing conditions make the Arctic more accessible to ships, with new waterways allowing improved access for oil and gas extraction, mining, fishing and tourism. Two major cargo-shipping routes are becoming viable: the Northwest Passage (NWP) and the Northern Sea Route (NSR), alternatives to the Panama and Suez canals to connect Europe, Asia and America. Compared with current routes, both new routes can reduce travel distance by up to 40%, leading to substantial fuel, cost, time and emission savings [2], as illustrated in Figure 1.

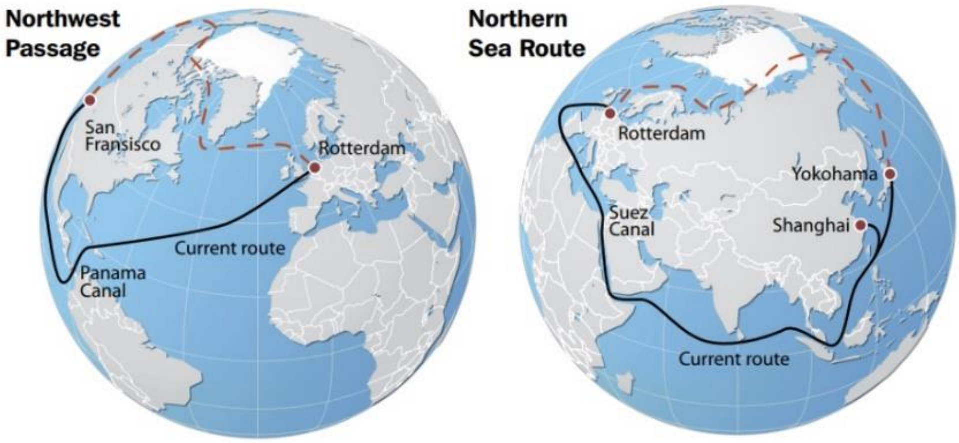

Figure 1: Comparison between the Arctic shipping routes (red dashed line) and the traditional shipping routes (solid black line) [3]

The practicality for employing the NSR is currently greater than for the NWP. As introduced by Ryan et al. [4], the NWP is made up of straits through the Canadian Arctic Archipelago that are both narrow and shallow. These straits are easily clogged by free floating ice, and are still insufficiently surveyed, presenting the very real risks of grounding or becoming stuck in ice; By contrast, the NSR presents a less complex situation, yet has several choke points where ships must pass through shallow straits between islands and the Russian mainland. Apart from the geographical factor, politics has also been providing increasing impetuses for adopting the NSR; for example, China has indicated its plans to establish a Polar Silk Road as part of the Belt and Road Initiative [5], which aims to build infrastructure and perform voyages through the NSR. There are four typical sub-passages in the NSR, as outlined in Figure 2, i.e. coastal route, middle route, high-latitude route and transpolar route. During the summer there is normally no ice appearing along the coastal or the middle line. Even in winter, the sea ice has significantly retreated in Kara and Barents seas [6–8].

Figure 2: Illustration of four typical sub-passages in the NSR: coastal route, middle route, high-latitude route and transpolar route [9]

The Arctic sea ice extent and thickness are seeing a continuous decline [10], with increasing navigable days for non-icebreaking vessels [11]. There have been a significant number of complete transits via the emerging Arctic sea routes. In 2019 alone, 24 and 35 ships transited through the NWP and NSR respectively, and there were over 2000 cargo voyages completed via segments of the NSR [12, 13]. Considering climate, economic and political factors, multiple predictive models have indicated an ongoing increase in the scale of vessels and voyages through these routes [14], and $1 trillion investment is planned for constructing infrastructure in the next 15 years to fulfil the needs of potential Arctic maritime operations [15]. These trends are attracting significant research interest in Arctic shipping, one aspect of which is to identify potential ice conditions and conduct corresponding ship design, power estimates and route planning.

Traditional polar ship design has focused on the level-ice condition, as the Arctic region tended to be covered by consolidated ice all year round and was only accessible to icebreakers. A large number of models have been developed to predict the level-ice resistance of ships [16–18]; in particular, significant recent progress has been made through high-fidelity computational modelling of the ice-breaking process, see Ni et al. [19], Li et al. [20, 21], Lilja et al. [22], and the review of Xue et al. [23]. Similar efforts have also been made to other traditional polar shipping scenarios, e.g. brash ice [24, 25] and ice ridges [26, 27]. The above models have been applied in practice and evolved into empirical equations and international guidelines, such as the Finnish-Swedish Ice Class Rules (FSICR) [28].

On the other hand, completed Arctic voyages in recent years have reported very different conditions from the traditional level, brash or ridge ice. The emerging shipping routes are observed to be infested by broken ice floes, especially during the summer season [1]. These floating floes range in sizes and only partly cover the sea surface. In addition, those floes tend to be circular due to the effect of wave wash and floe–floe collisions [14, 29, 30], as shown in Figure 3. Because of the flat, round appearance, this ice feature is commonly known as pancake ice. Figure 4 demonstrates the ice-floe condition (green and blue) along Arctic shipping routes, reported by field observations in the autumn of 2015, while level ice (red) occupies a small portion. With global warming, it can be anticipated that the proportion of ice-floe conditions will continue increasing, and the average size of floes will decrease. However, in the first half of the twenty-first century the shipping season will remain variable and unreliable [31]. Ship operations through level ice and ice ridges will remain important, as such challenging ice conditions will provide safety concerns for polar ships. Accordingly, almost all contemporary design standards and safety studies for marine structures are still based on the level ice condition [32, 33].

The operating limit of a ship in ice can refer to the Ice Class. During ship design, an Ice Class may be assigned according to the hull structural and machinery installation, which suggests a safe magnitude of equivalent ice thickness (ice thickness times ice concentration) that the ship may operate in. The relationship between Ice Class and intended equivalent ice thickness for operation is given in Table 1. In other words, with suitable ice-strengthening, a commercial ship can navigate in the emerging ice-floe without ice-breaking capabilities. This is making the ice-floe condition become a principal scenario of future Arctic shipping.

Table 1: Rules and Regulations of the Lloyd's Register - Ice Class and the Intended Equivalent Ice Thickness for Operation [34]

Ice Class	**Equivalent ice thickness (m)**
1AS	1.0
1A	0.8
1B	0.6
1C	0.4

Figure 3: A ship advancing in floating ice floes (photo credit: Alessandro Toffoli)

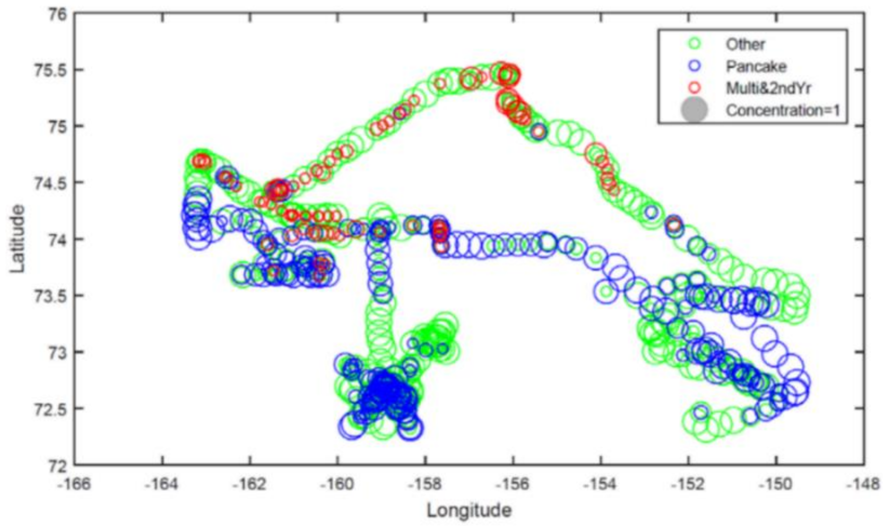

Figure 4: Ice floes (pancake and other) observed as the primary environment of shipping routes in West Arctic [1]

The process of a ship advancing in floating ice floes can be summarised as the following ship-wave-ice interaction: ship advancement generates waves; waves interact with ice floes; ice floes make contact with each other and with the ship [35–39]. In this scenario, ships tend to push the floes aside rather than break them [40], which means that the mechanism of ice resistance on the ship is very different from in level ice. In other words, existing resistance predictions for the level-ice condition may not be applicable for the emerging Arctic shipping conditions. For ship resistance in broken ice floes, Guo et al. [41] and Kim et al [42] conducted model tests to acquire data. Woolgar and Colbourne [43] presented regression analyses based on experimental data to derive the relationship of ice-floe load on a moored vessel with ice drift speed, ice friction, floe size and ice concentration. However, as their tests were conducted to study ice loads on a moored structure, the examined ice speed conditions are very small compared with normal shipping speeds, thus the relationships cannot be directly applied to ship resistance in ice floes. On the whole, relevant research on structures in floe ice is still very scarce [44], partially because the topic has only emerged recently, and also due to the prohibitive costs and complexity of ice experiments involving parameter matrices.

To provide a cost-effective solution to understand ship-wave-ice interaction and provide reliable resistance prediction, Huang et al. [45] developed a high-fidelity computational model using a combined CFD+DEM (Computational Fluid Dynamics and Discrete Element Method) approach that can simulate the operation of a ship in floating ice floes. This approach benefits from CFD that can obtain fully nonlinear fluid solutions, as well as DEM that can solve solid contacts to account for ship-ice collisions and ice-ice collisions. Two recent review articles of the field [23, 46] suggest that Huang et al. [45] is the first work that has coupled ship hydrodynamics with the ship-ice interaction process to achieve ship-wave-ice coupling. Experiments have confirmed the accuracy of this approach in predicting the ice-floe resistance. Moreover, ship and ice parameters such as hull form, ship speed and ice dimensions can be easily changed, thus allowing the consideration of extensive input combinations.

Despite the relative affordability of a computational approach, it may still be impractical to run a simulation each time a resistance estimate is needed. Therefore, there is the need to develop empirical equations for quick estimation of ice resistance for a given condition, so as to meet real-time purposes e.g. control system, decision support and training simulator [46–48]. One particular example is the Arctic Voyage Planning Tool (VPT). The VPT has the purpose of improving the safety and efficiency of cargo vessels operating in the Arctic, by optimising shipping routes in ice-infested waters [49]. Since the voyage planning process links with dynamic weather systems and works in real-time, it needs a rapid estimate of ice resistance for each potential route to provide decision-making support for the crew.

Therefore, following the development of the CFD+DEM model approach [45], the present work aims to develop a quick empirical equation to express ship resistance in ice floes and integrate it into VPT applications. This paper is organised as follows: Section 2 presents a systematic series of computational simulations for three different ships and for varying input conditions to identify the influential parameters for ship resistance in ice floes. Based on these simulation results, Section 3 proposes a non-dimensional derivation process, which is used to develop an empirical equation for ice-floe resistance. The derived equation is validated by multiple existing experiments. Section 4 introduces further applications of the rapid empirical equation, demonstrating how the equation is incorporated within a set of Arctic ship performance model and VPT that can predict ship fuel consumption in ice-infested waters and suggest shipping routes. In Section 5, the VPT incorporated with the derived equation is used to simulate a historical voyage and the predicted ship performance is validated against corresponding full-scale measurement data. Finally, Section 6 summarises this work with its implications. The design flow chart of this work is portrayed in Figure 5.

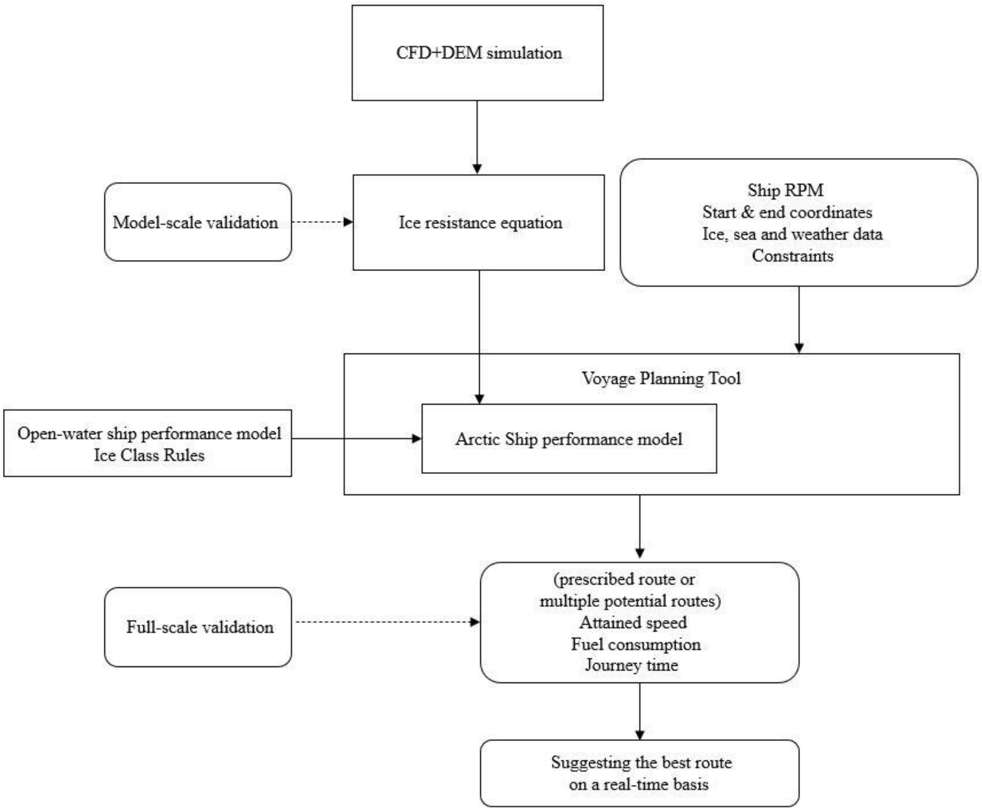

Figure 5: Design flow chart of this work

2. Candidate ships and computational modelling

Three ships are studied in this work: the KRISO Container Ship (KCS), the Japan Bulk Carrier (JBC), and a real Arctic In-service Vessel (AIV). These are three typical ship types that are expected to operate on future Arctic shipping routes, and they have significantly different hull forms that represent the diversity of current shipping fleets. Their dimensions and hull geometries are shown in Table 2 and Figure 6.

Table 2: Main Particulars of the Candidate Ships

	KCS	**JBC**	**AIV**
Ship type	Container ship	Bulk carrier	General cargo carrier
Length between perpendiculars [m]	230.0	280.0	186.4
Waterline beam [m]	32.2	45.0	28.5
Draught midships [m]	10.8	16.5	11.0
Block coefficient [-]	0.651	0.858	0.79
Wetted surface area [m^2]	9424.0	19556.1	8153.0

(a) Profile view

(b) Plan view

(c) Front view

Figure 6: Geometries of the KCS, JBC and AIV ships, in the order of KCS, JBC and AIV (image sizes correspond to the actual ship sizes)

These three ships were separately incorporated into the CFD+DEM model, as shown in Figure 7. The numerical theories and settings were detailly introduced in Huang et al. [45]. In brief, the CFD+DEM model consists of (a) a standard CFD model for ship advancement in open water that obtains fluid solutions, including the ship-generated wave; (b) a DEM used to model ice floes (assumed to be rigid bodies) and account for their collisions with the ship and nearby floes; these floes obtain fluid force from the CFD solution so that ship-wave-ice coupling is achieved; (c) original floe-distribution algorithms to import natural ice-floe fields into the CFD+DEM model, in which the floes are randomly distributed and have a range of sizes according to field measurements.

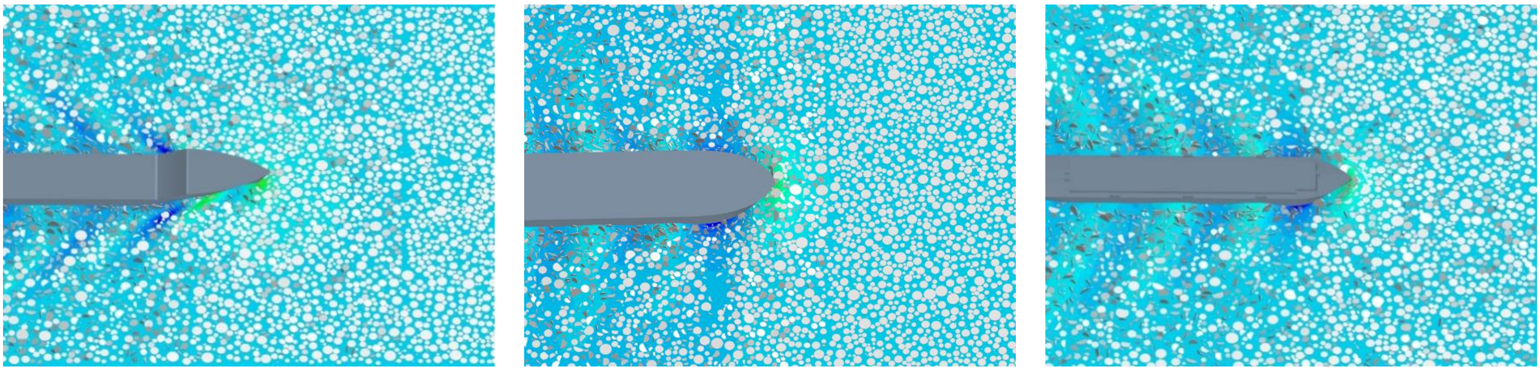

(a) KCS (b) JBC (c) AIV

Figure 7: Simulations of different ships advancing in ice floe fields

For each ship, systematic simulations were conducted to study relevant environmental variables, which is done by varying one parameter whilst holding others constant. The inserted hull geometries are in a model scale of 1:52.667, which was chosen to allow comparison of the simulations against model tests [41]. This process identified a series of influential parameters on ice floe resistance (R_{ice}): ship beam, ship speed, ice concentration, ice thickness and floe size, as introduced in Table 3.

The relationship of R_{ice} with these parameters is shown in Figures 8-12, with KCS taken as the example. In Figure 8-9 the ship speed and ice concentration were examined in sufficient ranges to obtain their regression powers, which are approximately 1.2 and 1.5. Similarly, the relationships of R_{ice} with ship beam, ice thickness and floe size were found to be linear, as plotted in Figures 10-12. These regression powers obtained for KCS do not have a notable difference from those obtained for JBC and AIV.

Table 3: Essential Variables for R_{ice}

Parameter	Definition	Symbol	[unit]
Ship beam	Maximal width on the ship's design waterline	B	[m]
Ship speed	Straight-line speed (can be converted to Froude number Fr $= \mathrm{U}/\sqrt{g \times L_{pp}}$, where g is gravitational acceleration)	U	[m*s^{-1}]
Ice concentration	The proportion of a certain sea surface covered by ice	C	[-]
Ice thickness	The average thickness of all floes	h	[m]
Ice diameter	The equivalent diameter of the ice upper surface	D	[m]

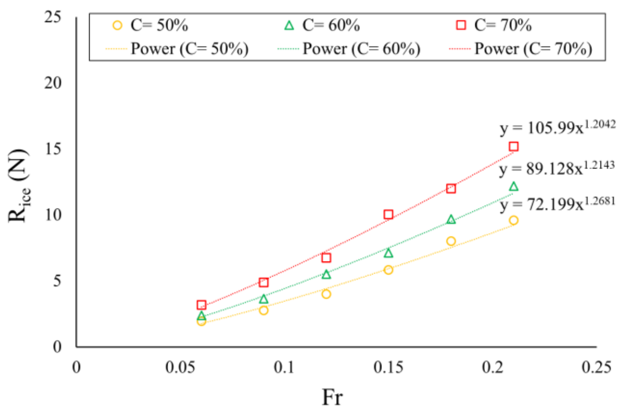

Figure 8: Ice-floe resistance for varying ship speed, obtained when h = 0.02 m; results of 1:52.667 KCS hull model

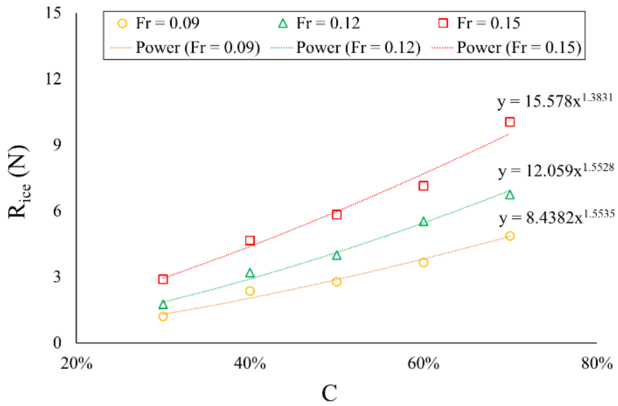

Figure 9: Ice-floe resistance for varying ice concentration, obtained when *h* = 0.02 m; results of 1:52.667 KCS hull model

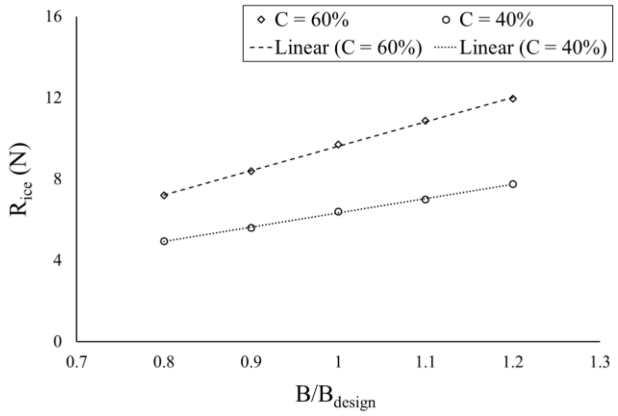

Figure 10: Ice-floe resistance as a function of ship beam (normalised by the designed beam), obtained when Fr = 0.18 and *h* = 0.02 m; results of 1:52.667 KCS hull model

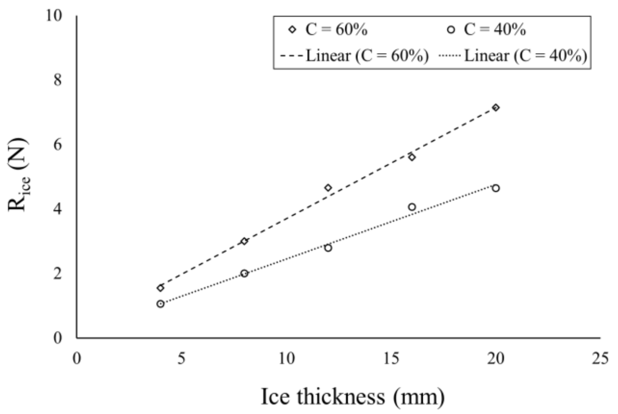

Figure 11: Ice-floe resistance for varying ice thickness, obtained when Fr = 0.15; results of 1:52.667 KCS hull model

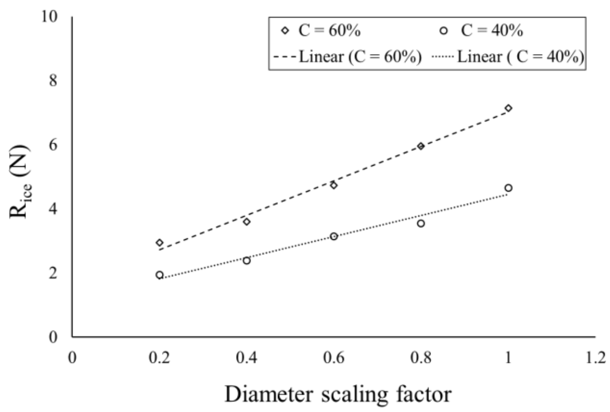

Figure 12: Ice-floe resistance as a function of floe size, obtained when Fr = 0.15 and h = 0.02 m; results of 1:52.667 KCS hull model. The diameter scaling factor denotes a value to be multiplied by all floe diameters applied in the experiments of [41].

3. Derivation of an empirical equation for ice-floe resistance

This section starts by introducing a non-dimensional procedure to derive a rational expression of R_{ice}, based on the principal parameters and regression powers identified in the previous section. Subsequently, the ice resistance equations for the three different ships are derived, and their differences are discussed to further derive a generic equation to account for different ships. Then, the derived generic equation is validated by predicting ice resistance for previous experimental conditions. Furthermore, a discussion is given on the extrapolation of the equation from model-scale to full-scale.

3.1 Non-dimensional analysis

R_{ice} is first expressed using parameters shown in Table 3. This gives:

$$R_{ice} = A \times \rho_{ice}{}^{a} \times h^{b} \times D^{c} \times U^{d} \times \mathrm{B}/L_{pp}{}^{m} \times C^{n} \qquad (1)$$

where A is a coefficient dependent on the specific ship, and ρ_{ice} is the ice density used for matching up the units between the left- and right-hand sides of the equation. Subsequently, using a standard non-dimensional method to fit the units of both sides, it gives: a = 1, b + c = 2 and d = 2, thus,

$$R_{ice} = A \times \rho_{ice} \times h^{b} \times D^{c} \times U^{2} \times \mathrm{B}/L_{pp}{}^{m} \times C^{n} \qquad (2)$$

Based on the regression powers shown for h, D, B and C, b = 1, c = 1, m = 1 and n = 1.5. Since the power of speed was found to be 1.2, while its unit-based power is 2, a non-dimensional parameter Froude number ($\mathrm{Fr} = \mathrm{V}/\sqrt{g \times L_{pp}}$) is introduced to fulfil both the power and unit; thereby the power of Fr derives to be -0.8, therefore:

$$R_{ice} = A \times \rho_{ice} \times h \times D \times U^2 \times \mathrm{B}/L_{pp} \times C^{1.5} \times Fr^{-0.8} \tag{3}$$

In reality, ice floes in a given region are of different dimensions, where h has little variation while D of floes can be notably different. Thus, it is recommended to input a constant h and calculate an average D for the equation based on an average Aspect Ratio (AR), i.e. $D = h \times \mathrm{AR}$. Field measurements reported that a generally applicable average value for AR is 10 for ice floe fields [50]. The density of the ice, ρ_{ice}, can be held constant at 900 kg/m^3.

Then, the parameters of KCS, JBC and AIV hulls were inserted in Equation (3) to find the corresponding A values. This in turn gives $A_{KCS} = 7.64$, $A_{JBC} = 11$ and $A_{AIV} = 5.5$. These coefficients can be inserted in Equation (3) to provide relatively accurate predictions for ice-floe resistance, as shown in Figures 13-15.

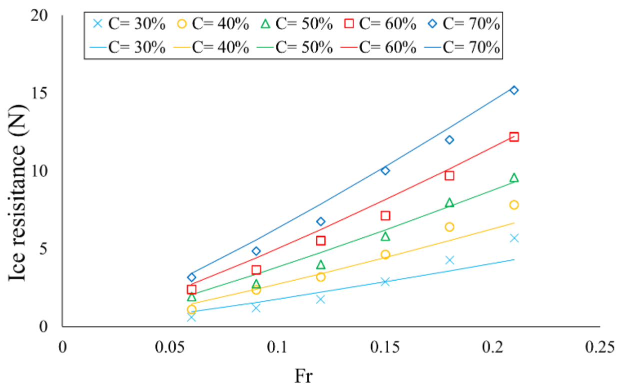

Figure 13: Ice-floe resistance calculated by simulations (symbols) and Equation (3) (lines), when h = 0.02 m; results of 1:52.667 KCS hull model

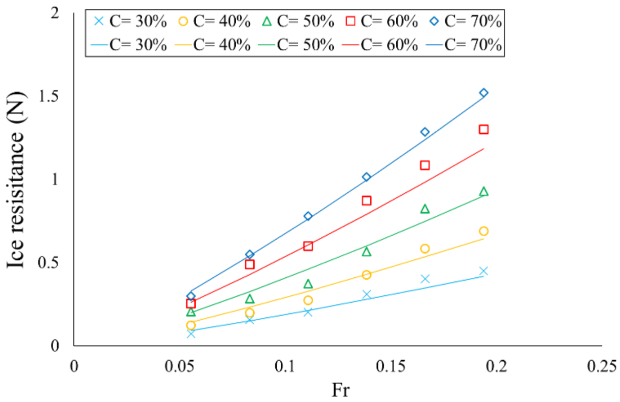

Figure 14: Ice-floe resistance calculated by simulations (symbols) and Equation (3) (lines), when h = 0.0066 m; results of 1:52.667 JBC hull model

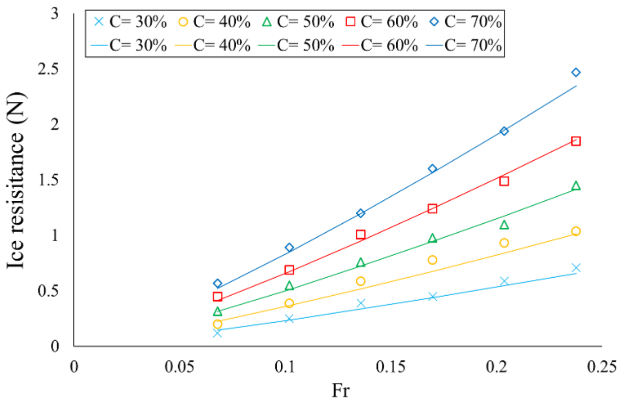

Figure 15: Ice-floe resistance calculated by simulations (symbols) and Equation (3) (lines), when h = 0.0066 m; results of 1:52.667 AIV hull model

3.2 Unification for multiple hull forms

Equation (3) has accounted for the influence of ship beam, while other parameters of the hull geometries still make the ice resistance coefficients different for each of the three ships. To investigate the underlying reasons and derive a generic equation, the ship-wave-ice interactions of these three hulls were further analysed, by which, two influential bow parameters were identified: buttock angle (γ) and waterline angle (α), which are illustrated in Figure 16.

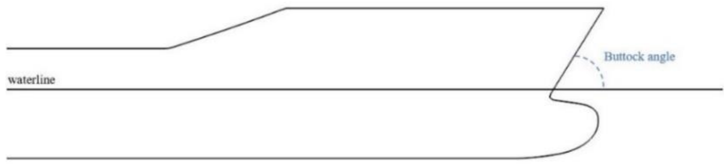

(a) Central plane of the KCS hull

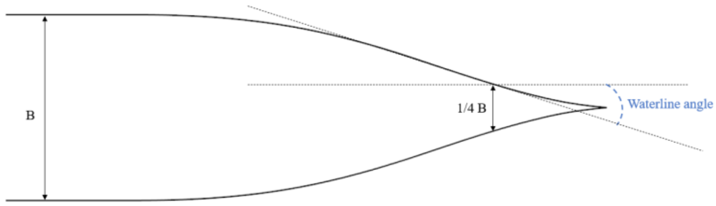

(b) Waterline plane of the KCS hull

Figure 16: Graphic expression of buttock angle and waterline angles, defined following the International Association of Classification Societies [51]

The buttock angle mainly influences the ship-wave-ice interaction in the vertical direction. It may be observed in Figure 6(a) that the bow of KCS or JCS has a buttock angle of approximate 60°, while the AIV has a vertical stem, i.e. buttock angle is 90°. The buttock angle dictates the contact surface between the ship and floes, which influences the ice resistance.

The waterline angle mainly influences the ship-wave-ice interaction in the transverse direction. The KCS has a sharp bow shape across the waterline, while JBC and AIV have relatively round shapes across the waterline. The round shape tends to generate a wave profile that pushes ice floes aside from the ship, as shown in Figure 17. This wave profile results in a reduction in the ice resistance.

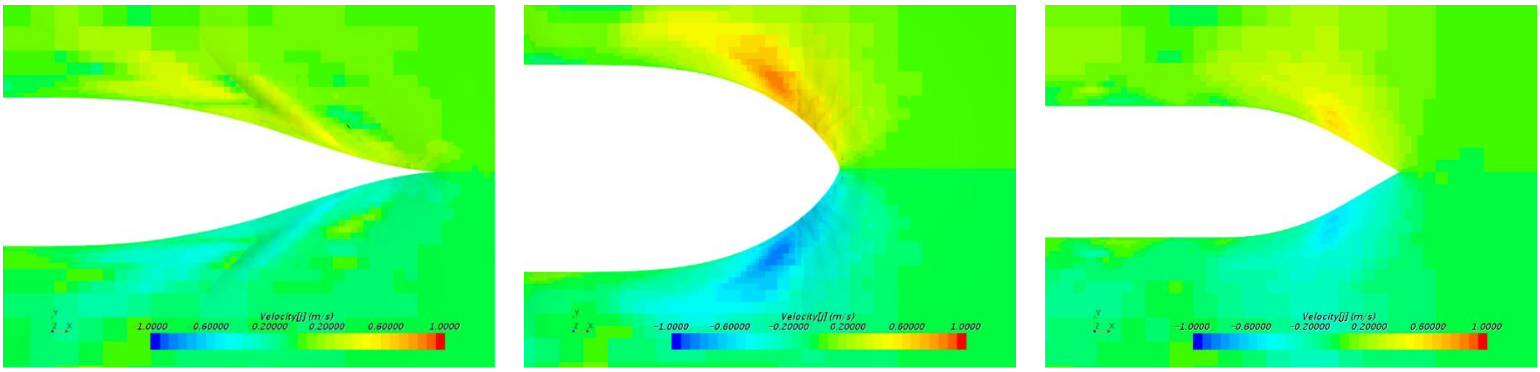

(a) KCS (b) JBC (c) AIV

Figure 17: Waterline velocity fields around the bows, colour contours show the velocity magnitude in the transverse direction

Table 4: Bow Angles of the Candidate Ships and the Corresponding R_{ice} Coefficients in Equation (3)

	KCS	**JBC**	**AIV**
Buttock angle (γ) [degrees]	58	61	90
Waterline angle measured at 1/4 beam (α) [degrees]	18	50	30
Calculated ice floe resistance coefficients [-]	7.64	5.5	11

To unify the ice-floe equation for multiple hull forms, the bow angles of KCS, JBC and AIV were measured and shown in Table 4. γ and α are required to be inserted in Equation (3) to account for their influences. The influence of buttock angle on the ice-induced resistance force on ships was discussed by Riska et al. [18], where the authors note that, for icebreaking vessels, R_{ice} tends to be proportional to the tangent of γ, but their extensive experience shows that the influence of γ on R_{ice} is less dominating than a tangent function for non-icebreaking vessels; thus, γ is instead taken to have a unit-power correlation with R_{ice}. After normalising a unit power of γ against the ice-resistance coefficients for the three ships, the reduction effect of α on R_{ice} is shown to be a cosine function. Therefore, Equation (3) becomes:

$$R_{ice} = 0.13665 \times \gamma \times \cos\alpha \times \rho_{ice} \times h \times D \times U^2 \times \mathrm{B}/L_{pp} \times C^{1.5} \times Fr^{-0.8} \qquad (4)$$

Equation (3) and Equation (4) provide identical results, while Equation (4) is applicable for all the three investigated ships without requiring the calculation of a specific coefficient for a specific vessel. Following the same approach, further parameters and relationships could be identified when more data becomes available in future work.

The uncertainty of the derivation process is analysed through nondimensionalising R_{ice} by parameters of Equation (4). As shown in Figure 18, most of the nondimensionalised R_{ice} lays in a range of $0.13665 \times (1 \pm 15\%)$, which indicates the inherent residual. The residual is expected due to the nature of empirical derivation, and the 15% level has made an improvement than previous work (e.g. Figure 19 of Guo et al. [41]) by including more parameters that were not considered in previous simpler ice-floe resistance derivation. However, the residual could be further reduced by applying advanced machine learning algorithms [52–54]. When predicting ship fuel consumption of an ice-infested route, the uncertainty level is expected to be less than 15% as highly variable ice conditions should offset the residual of each other.

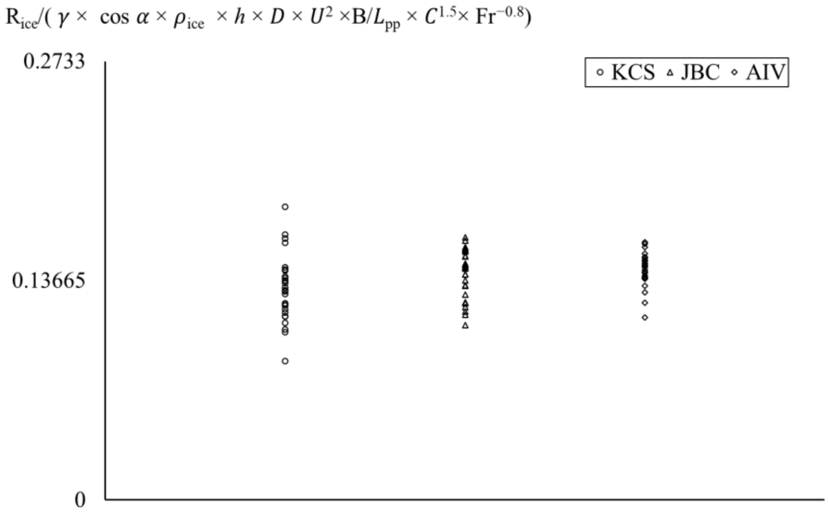

Figure 18: R_{ice} data from simulations nondimensionalised by the parameters of Equation (4)

3.3 Validation

The equation to predict ice-floe resistance was validated against two sets of model tests with different hull, ice and speed conditions:

Firstly, Equation (4) was used to provide prediction against experiments conducted in the towing tank of Harbin Engineering University in China [41], where a model-scale KCS hull was towed through a field of numerous pieces of floating paraffin wax, mimicking rigid ice floes. The floe resistance was interpreted as being the total ship resistance in floes minus the corresponding calm water resistance without floes. To make the comparison, Equation (4) was directly inputted with the same ship, ice, operating parameters used in the experiments, where the ship speed ranges from Fr = 0.03 to 0.18, ice concentration ranges from C = 60% to 90%, and ice thickness h = 0.02 m. The comparison between computational and experimental results is presented in Figure 19, where Equation (4) is shown to be fairly accurate and the deviations are reasonably within the range of derivational and experimental uncertainties.

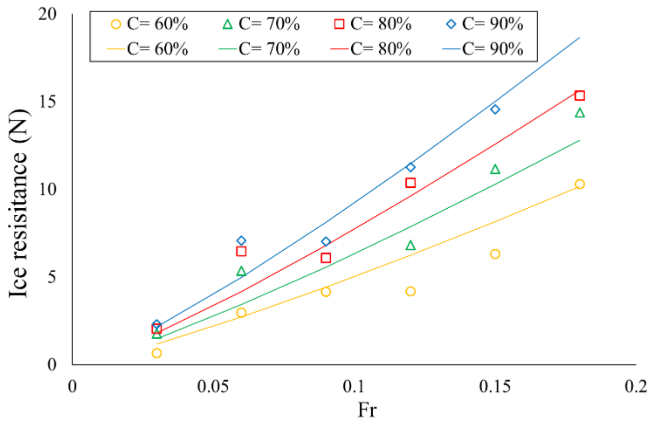

Figure 19: Comparison between ice-floe resistance of 1:52.667 KCS hull model measured by experiments [41] (symbols) and calculated by Equation (4) (lines)

To further confirm the accuracy of Equation (4), another set of experiments were found that were recently conducted in the Korea Research Institute of Ships and Ocean Engineering [42]. Towing tests were carried out in laboratory ice floes for a model-scale Araon ship whose hull form considerably differs from the three hulls studied earlier, as shown in Figure 20. Equation (4) was directly inputted with the same ship, ice, operating parameters that used in the experiments, where the ship speeds are Fr = 0.017, 0.05 and 0.084, ice concentrations are C = 60% and 80%, and ice thickness h = 0.057 m. The comparison presented in Figure 21 shows good agreement; in particular, this demonstrates that the derived equation can be applicable to other hull shapes, speeds, and ice conditions that were not considered in the derivation process.

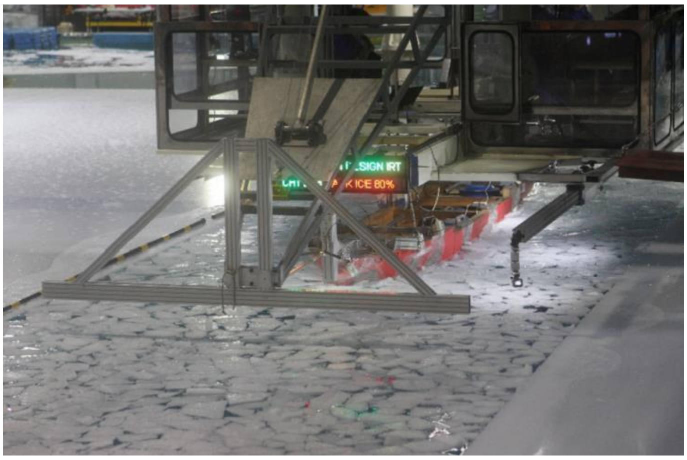

Figure 20: Ice model tests of 1:18.667 Araon hull model reported by Kim et al. [42]

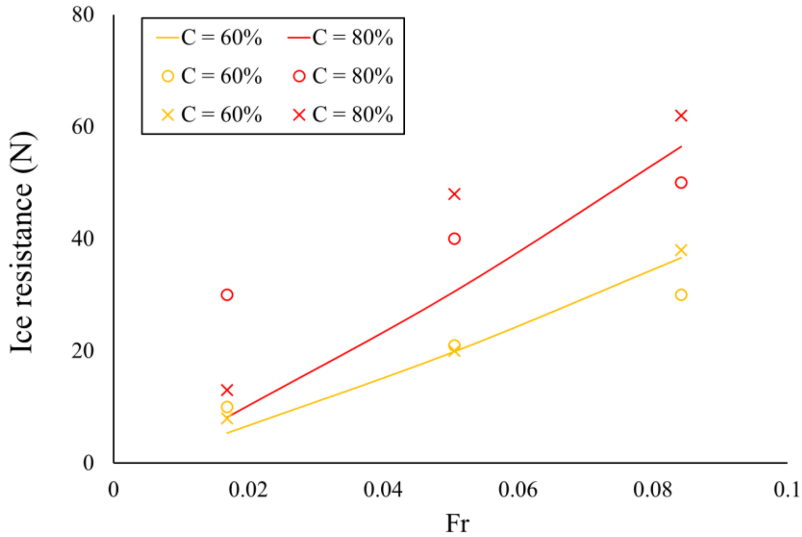

Figure 21: Comparison among ice-floe resistance of 1:18.667 Araon hull model given by Equation (4) (lines), by experiments (circles) and by the finite-element method (crosses) of Kim et al. [42]

For the lowest speed and C = 80% in Figure 21, it may be seen that the experimental resistance is significantly larger than that predicted by Equation (4). Kim et al. [42] indicate that this test condition could be a special case, as the experimental value is also much higher than that predicted by their finite-element model. It is expected that R_{ice} should equal 0 when Fr = 0, while the experimental R_{ice} is approximate 30 N when Fr is very small at 0.017 and the slope would lead to a clearly unphysical R_{ice} (larger than 20 N) even when Fr = 0. The same phenomenon is discussed by Riska et al. [18], where they indicated that at very low speeds ships cannot proceed continuously in ice towing tanks, thus the measured average towing force is not directly applicable to the prediction of R_{ice}.

In addition, noting that the floe shape is circular in Huang et al. [45], square in Guo et al. [41], and an irregular polygon in Kim et al. [42], the coincident trends and agreement among these works indicate that floe shape may not be a critical parameter for the ice resistance of the studied conditions.

3.4 Full-scale extrapolation

The computational modelling was conducted at model scale to allow validation against experiments, so it is important to discuss how the derived R_{ice} equation can be applied to full-scale ships. For water resistance (R_{water}), the derivation of formulae from model tests usually needs to apply the ITTC extrapolation procedure [55], since it is impossible to ensure Froude and Reynolds numbers are both equal in full scale and model scale, in which, the former governs gravity/inertia (waves) forces and the latter governs viscous forces. R_{water} can be divided into a wave component and a frictional component; in model tests, scaling based on a consistent Froude number is practical, which scales the wave component correctly yet brings about certain errors within the friction component due to changes in Reynolds number. The latter may be corrected using the ITTC method [55].

Similarly, for the extrapolation of ice resistance, Froude and Cauchy numbers should be both equal between full scale and model scale, otherwise a correction procedure would also be required [56]; Cauchy number relates to the elasticity of ice, whose consistency is for the elastic reaction forces of ice are correctly scaled, which is essential to accurately represent the icebreaking process. However, in the present ice-floe case, in principle the small floes are pushed away rather than broken by the ship, so the floes can be assumed to be rigid [40], thus the Cauchy number is infinitely small in both scales and relevant corrections do not need to be applied. Therefore, the present work proposes that Equation (4) can be directly applied to full scale, as the non-dimensional derivation has already kept the expression in line with Froude's law. However, it should be noted that this is a theoretical inference, and future validation is still required to prove the applicability of scaling the ice-floe resistance equation from model-scale to full-scale.

4. Application

The achievement of Equation (4) is providing a rapid estimate of ice-floe resistance for a given ship in a given ice condition, which in turn enables its incorporation into real-time applications. The derived ice-floe resistance equation has already been incorporated into a new Arctic Ship Performance Model (ASPM) and VPT, as presented in Li et al. [57] (in which the ASPM was named SPM-B). Hence, only the most salient points are recounted in this section.

4.1 Arctic ship performance model

The calculation procedure of the ASPM is given in Figure 22. It can be seen that most of the procedure can be completed using classical naval architecture methods [58–60], whilst an essential addition is the calculation of added resistance due to ice. In the ASPM, ice resistance is classified into large ice floes and small ice floes. These two conditions correspond to significantly different physics during the ship-ice interactions. Large ice floes undergo crushing and break-up when ships are operating through them, and the ultimate of this case is level ice. By contrast, small ice floes have a high degree of freedom, thus their response to ships is mainly being pushed away rather than fractured. Extreme ice conditions, such as ice ridges, are not considered in the ASPM, since they are designed to be detected by the crew and avoided during operations. Therefore, two different methods were required to account for the ice resistance in large and small ice-floe scenarios, for which the ASPM respectively incorporated the empirical method provided by FSICR using the equivalent ice thickness [61] and Equation (4) derived in the present work. After incorporating ice-resistance equations, the ASPM has the capability of predicting the fuel consumption and attained speed for ships navigating in ice-infested routes. The threshold between large and small floes in the current ASPM is C × h = 0.3 m, which is based upon the classification of UK Met Office that when C × h > 0.3 m first-year ice starts to grow and ship-induced fracture is expected occur, and when C × h ≤ 0.3 m ice types are young grey, pancake and grease floes that do not expect ship-induced fracture [62].

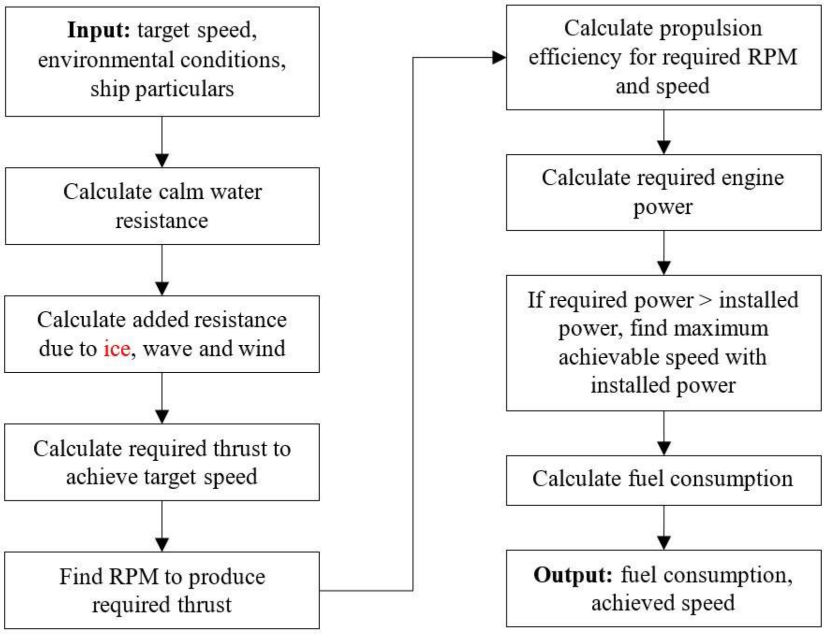

Figure 22: Calculation procedure of the Arctic Ship Performance Model

4.2 Arctic voyage planning tool

The ASPM was integrated into a VPT [49], which links with real-time weather and ice forecasting systems to calculate a ship's fuel consumption along all potential routes. Then the VPT performs two steps to determine the optimal route: (a) eliminate any route that contains an ice condition to violate the POLARIS standard to cause a structural risk [63] (b) suggest the route with the least fuel consumption. The coupled weather systems include the Copernicus Marine Environment Monitoring Service that provides metocean data and the UK Met Office Forecast Ocean Assimilation Model that provides sea ice data [62]. Figure 23 provides two examples of suggested routes for a ship travelling through the Northern Sea Route, obtained using the VPT based on historical metocean and ice data in 2018. In Figure 23(a), it can be seen that the majority of the Arctic was covered by sea ice at that time (early summer), and the VPT chose a route close to the Russian coastline, where the ice conditions were not severe (referred to as coastal route in Figure 2); in Figure 23(b), the Arctic sea ice reached the annual minimum (late summer), and the VPT chose a shorter route via the higher-latitude Arctic Ocean (referred to as high-latitude route in Figure 2). These route choices show the VPT can minimise the ship fuel consumption based on a comprehensive consideration of shorter voyage distance and less ice impact, which signifies its practical value to Arctic shipping. Nonetheless, the shown examples are for the summer season, and intended future work is to study the VPT application in winter scenarios, in which the ice impact will be more significant as will be the benefit of route planning.

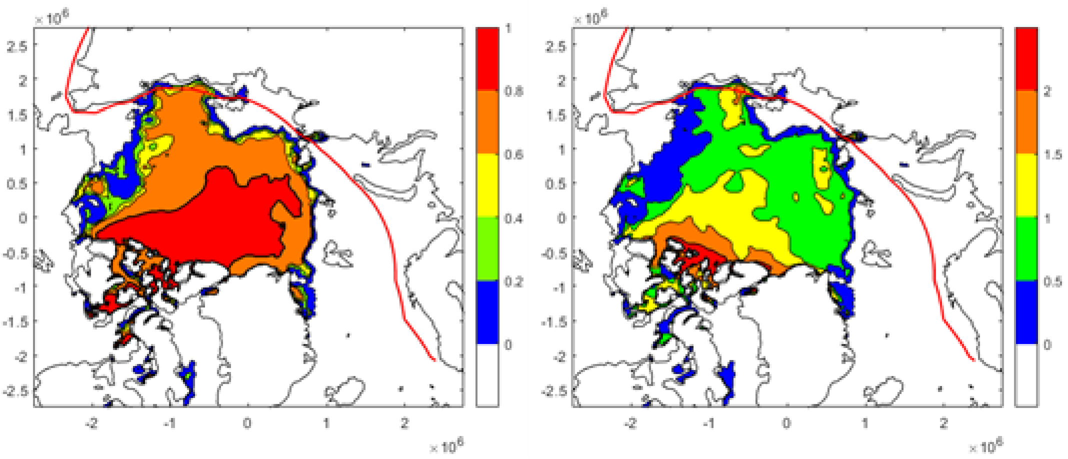

(a) 20 July 2018 - 15 August 2018, when the majority of the Arctic was covered by sea ice

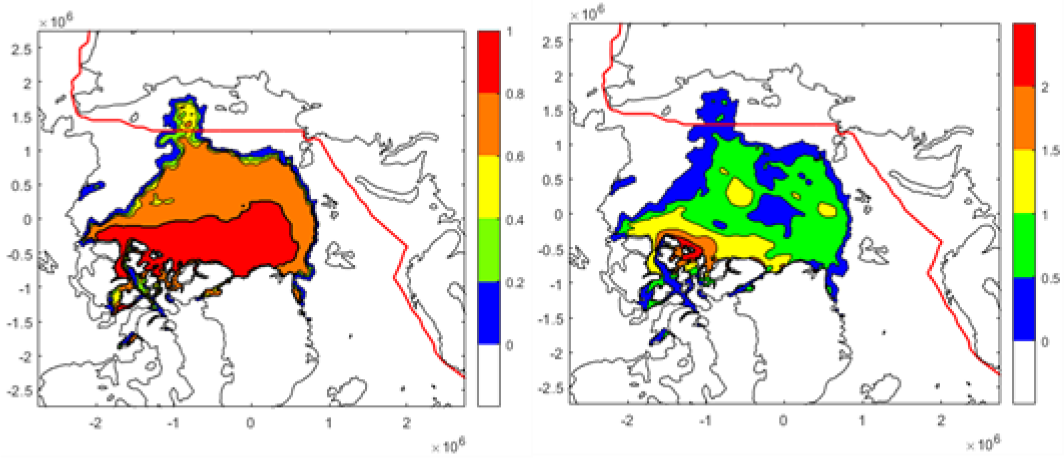

(b) 01 September 2018 - 24 September 2018, when Arctic ice was the least of the year.

Figure 23: Two VPT-suggested routes for a ship travelling through the Northern Sea Route, obtained using the metocean and ice data of early & late summer 2018. Colour bars denote ice concentration in the left panels and ice thickness (meter) in the right panels, and the *x* and *y* axes denote the distance (meter) with respect to the North Pole origin

It is seen in Figure 23(a) that the ice thickness exceeds 1.5 m along a small segment of the route. In practice, icebreakers may be required to create a channel so that a commercial ship can transit through such thick ice. To account for this, the VPT now has a function to switch into “icebreaker-assistance mode” when the ice is sufficiently thick, as reported in Li et al. [64].

5. Comparison with full-scale measurements

Full-scale measurements were collected for the real AIV ship during a voyage through a segment of NSR near the East Siberian Sea. The data were recorded from 03:00 AM 05/08/2018 to 11:30 PM 07/08/2018. The ship's central computer recorded the ship's engine RPM, GPS position, encountered wind speed and direction, and attained speed. The encountered sea ice concentration was collected by the onboard cameras that were specifically equipped for sea ice monitoring. Figure 24 plots the measured RPM and ice concentration along the voyage. The figure shows that the RPM was first manually reduced by the crew, before the ship entered the ice-floe field, which was to slow and protect the ship. After the ship entered the ice floe field, the RPM increased due to the additional ice resistance and fluctuated with the variation of ice condition. After the ship passed by the ice-floe field, the RPM was manually increased to speed up the ship in open water.

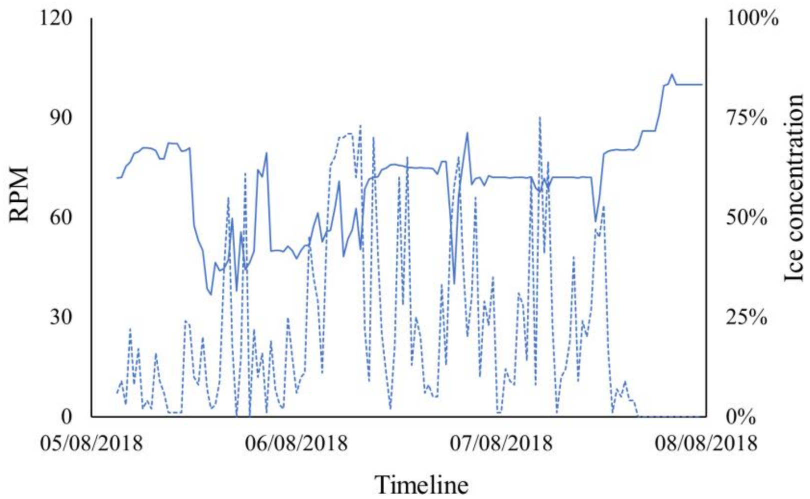

Figure 24: Full-scale measurement of engine RPM (solid line) and sea ice concentration (dashed line).

This particular voyage was replicated using the ASPM and VPT. The inputs included (a) the onboard recorded ice concentration, wind data and ship RPM; (b) ice thickness that was inputted from historical satellite data of the UK Met Office, where the ice thickness did not show a notable variation along the voyage, thus a constant value of 0.35 m was taken, which is the average of the encountered sea ice thickness; (c) the historical metocean data from the Copernicus Marine Environment Monitoring Service, which includes waves and currents. Throughout the whole voyage, the encountered sea ice was observed to be small ice floes that have negligible ship-induced fracture; therefore the ice resistance was calculated by Equation (4) rather than FSICR.

Using the ASPM and VPT, the ship was set to sail at the measured RPM following the same route as that recorded by the GPS. Based on the inputs of the environmental variables, Equation (4) and open-water ship resistance equations were used to calculate the variation of ship total resistance along the route. Then, the predicted total resistance is combined with the RPM and propulsion system (Table 5) to calculate the attained speed and fuel consumption of the ship. The measured ship speed was compared with the predicted value in Figure 25. The comparison shows good agreement, justifying the rationality of using Equation (4) to account for ice-floe resistance in such a VPT application.

This example presents a workable approach that uses the derived ice-floe equation to rapidly predict ship performance in ice-infested seas, which meets relevant engineering requirements for a real-time application. Nonetheless, it should be noted that this full-scale validation has only been performed against a three-day voyage, due to the scarcity of available data containing ice-floe conditions. A complete validation procedure for a mature ice-floe equation will need more field and experimental data to help confirm its accuracy.

Table 5: Particulars of the Propulsion System of AIV.

Main engine	WinGD 6RT-flex50-D
Maximum Continuous Rating (MCR)	10,470kW * 124 r/min
Continuous Synopsis Record (CSR = 65% MCR)	6,806 kW * 107.4 r/min

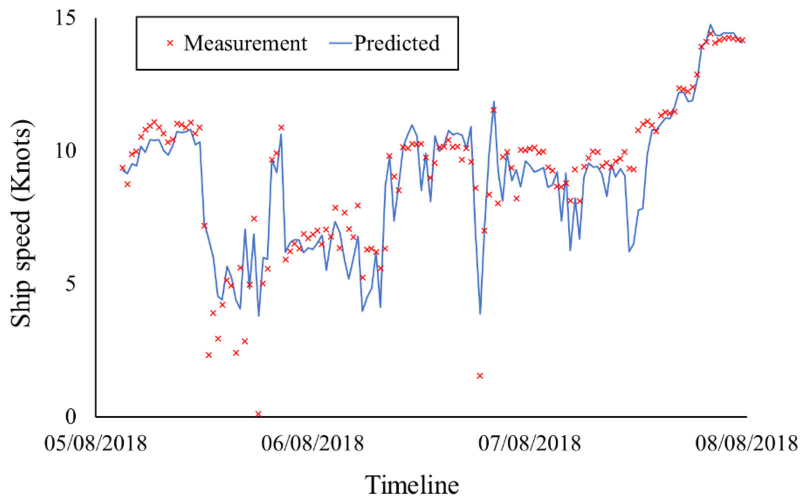

Figure 25: Predicted ship speed against full-scale measurements.

6. Conclusions

The recent reduction in Arctic sea ice has resulted in increased navigability for commercial ships, whilst also presenting a new environmental condition – floating ice floes. Addressing this emerging scenario, this work provides a computationally cheap empirical equation for predicting ship resistance when operating in such floes. Based upon extensive computational simulations and analyses, the equation explicates how the ice resistance is related to hull, speed and ice parameters, providing valuable insights for polar ship design and engine power estimation. In particular, the influences of buttock and waterline angles were investigated.

Furthermore, the derived equation enables the quick prediction of ice-floe resistance on a given ship in given ice conditions, which has facilitated the development of an Arctic ship performance model and voyage planning tool. These applications reveal significant practical value through demonstrating the ability to estimate fuel consumption for ice-going ships and suggest their routes on a real-time basis.

Validation against both model-scale and full-scale results demonstrate the rationality of the non-dimensional derivation procedure and the accuracy of the proposed ice resistance equation. However, since available experimental and field data on the present problem are still scarce, there could be extra parameters and relationships of the equation to be identified, as more data becoming available in the future.

Acknowledgements

This work is part of a project that has received funding from the European Union's Horizon 2020 research and innovation programme under grant agreement No 723526 - SEDNA: Safe maritime operations under extreme conditions; the Arctic case. The authors would like to thank Andrea Grech La Rosa for his assistance on the applied hull forms.

References

[1] J. Thomson, S. Ackley, F. Girard-Ardhuin, F. Ardhuin, A. Babanin, G. Boutin, J. Brozena, S. Cheng, C. Collins, M. Doble, Overview of the arctic sea state and boundary layer physics program, Journal of Geophysical Research: Oceans. (2018).

[2] L.C. Smith, S.R. Stephenson, New Trans-Arctic shipping routes navigable by midcentury, in: Proceedings of the National Academy of Sciences, 2013: pp. E1191–E1195.

[3] A. Monitoring, Changes in arctic snow, water, ice and permafrost. swipa 2011 overview report, Arctic Climate. (2012).

[4] C. Ryan, G. Thomas, D. Stagonas, Arctic Shipping Trends 2050, University College London, 2021.

[5] Y. Peng, Z. Li, W. Duan, X. Li, Q. Bao, Evolution of the hinterlands of eight Chinese ports exporting to europe under the Polar Silk Road: Three hypothetical scenarios, Ocean & Coastal Management. 205 (2021) 105549.

[6] W.N. Meier, J. Stroeve, F. Fetterer, Whither Arctic sea ice? A clear signal of decline regionally, seasonally and extending beyond the satellite record, Annals of Glaciology. 46 (2007) 428–434.
[7] I.H. Onarheim, M. \AArthun, Toward an ice-free Barents Sea, Geophysical Research Letters. 44 (2017) 8387–8395.
[8] C. Duan, S. Dong, Z. Xie, Z. Wang, Temporal variability and trends of sea ice in the Kara Sea and their relationship with atmospheric factors, Polar Science. 20 (2019) 136–147.
[9] K. Si, China to launch communication test in Northern Sea Route, Seatrade Maritime News. (2021).
[10] J.-C. Gascard, K. Riemann-Campe, R. Gerdes, H. Schyberg, R. Randriamampianina, M. Karcher, J. Zhang, M. Rafizadeh, Future sea ice conditions and weather forecasts in the Arctic: Implications for Arctic shipping, Ambio. 46 (2017) 355–367.
[11] V.C. Khon, I.I. Mokhov, M. Latif, V.A. Semenov, W. Park, Perspectives of Northern Sea Route and Northwest Passage in the twenty-first century, Climatic Change. 100 (2010) 757–768.
[12] R.K. Headland, Transits of the Northwest Passage to end of the end of 2019 navigation season, Scott Polar Research Institute. (2019).
[13] Nord University, Overall NSR voyages statistics distributed by Ice class, number of voyages and GRT., Northern Sea Route Information Office. (2019).
[14] P. Wadhams, A farewell to ice: a report from the Arctic, Oxford University Press, 2017.
[15] S. Minerd, Sustainable Development: The Future of Investing, In Proceedings of Milken Institute Global Conference. (2016).
[16] E. Enkvist, On the ice resistance encountered by ships operating in the continuous mode of icebreaking, 1972.
[17] A. Lindquist, Straightforward method for calculation of ice resistance of ships, POAC'89. (1989).
[18] K. Riska, M. Wilhelmson, K. Englund, T. Leiviskä, Performance of Merchant vessels in the Baltic, Ship Laboratory, Winter Navigation Research Board, Helsinki University of Technology, Espoo, Finland, Research Report. (1997).
[19] B.-Y. Ni, Z.-W. Chen, K. Zhong, X.-A. Li, Y.-Z. Xue, Numerical simulation of a polar ship moving in level ice based on a one-way coupling method, Journal of Marine Science and Engineering. 8 (2020) 692.
[20] F. Li, M. Kotilainen, F. Goerlandt, P. Kujala, An extended ice failure model to improve the fidelity of icebreaking pattern in numerical simulation of ship performance in level ice, Ocean Engineering. 176 (2019) 169–183.
[21] F. Li, M. Kõrgesaar, P. Kujala, F. Goerlandt, Finite element based meta-modeling of ship-ice interaction at shoulder and midship areas for ship performance simulation, Marine Structures. 71 (2020) 102736.
[22] V.-P. Lilja, A. Polojärvi, J. Tuhkuri, J. Paavilainen, Finite-discrete element modelling of sea ice sheet fracture, International Journal of Solids and Structures. 217 (2021) 228–258.
[23] Y. Xue, R. Liu, Z. Li, D. Han, A review for numerical simulation methods of ship–ice interaction, Ocean Engineering. 215 (2020) 107853.
[24] M. Mellor, Ship resistance in thick brash ice, Cold Regions Science and Technology. 3 (1980) 305–321.
[25] W. Luo, D. Jiang, T. Wu, C. Guo, C. Wang, R. Deng, S. Dai, Numerical simulation of an ice-strengthened bulk carrier in brash ice channel, Ocean Engineering. 196 (2020) 106830.
[26] H. Gong, A. Polojärvi, J. Tuhkuri, Discrete element simulation of the resistance of a ship in unconsolidated ridges, Cold Regions Science and Technology. (2019) 102855.
[27] H. Gong, Discrete-element modelling of ship interaction with unconsolidated ice ridges: ridge resistance and failure behaviour, PhD Thesis, Aalto University, 2021.
[28] M. Juva, K. Riska, On the power requirement in the Finnish-Swedish ice class rules, Winter Navigation Research Board, Res. Rpt. 53 (2002).
[29] G.-Y. Yuan, B.-Y. Ni, Q.-G. Wu, Y.-Z. Xue, A.-M. Zhang, An experimental study on the dynamics and damage capabilities of a bubble collapsing in the neighborhood of a floating ice cake, Journal of Fluids and Structures. 92 (2020) 102833.
[30] B.Y. Ni, Y.T. Pan, G.Y. Yuan, Y.Z. Xue, An experimental study on the interaction between a bubble and an ice floe with a hole, Cold Regions Science and Technology. 187 (2021) 103281.

[31] N. Melia, K. Haines, E. Hawkins, Future of the Sea: Implications from opening Arctic sea routes, Foresight–Future of the Sea Evidence Review. London: Government Office of Science. (2017).
[32] G.W. Timco, W.F. Weeks, A review of the engineering properties of sea ice, Cold Regions Science and Technology. 60 (2010) 107–129.
[33] C. Duan, S. Dong, Z. Wang, Estimates of Sea Ice Mechanical Properties in the Kara Sea, Pure and Applied Geophysics. 177 (2020) 5101–5116.
[34] L. Register, Rules and regulations for the classification of naval ships, England: Lloyd's Register. (2021).
[35] L.J. Yiew, L.G. Bennetts, M.H. Meylan, G.A. Thomas, B.J. French, Wave-induced collisions of thin floating disks, Physics of Fluids. 29 (2017) 127102. https://doi.org/10.1063/1.5003310.
[36] L. Huang, G. Thomas, Simulation of Wave Interaction With a Circular Ice Floe, Journal of Offshore Mechanics and Arctic Engineering. 141 (2019) 041302.
[37] L. Huang, K. Ren, M. Li, Ž. Tuković, P. Cardiff, G. Thomas, Fluid-structure interaction of a large ice sheet in waves, Ocean Engineering. 182 (2019) 102–111.
[38] L. Huang, M. Li, T. Romu, A. Dolatshah, G. Thomas, Simulation of a ship operating in an open-water ice channel, Ships and Offshore Structures. 16 (2021) 353–362. https://doi.org/10.1080/17445302.2020.1729595.
[39] Y.Z. Xue, L.D. Zeng, B.Y. Ni, A.A. Korobkin, T.I. Khabakhpasheva, Hydroelastic response of an ice sheet with a lead to a moving load, Physics of Fluids. 33 (2021) 037109.
[40] A. Polojärvi, J. Tuhkuri, O. Korkalo, Comparison and analysis of experimental and virtual laboratory scale punch through tests, Cold Regions Science and Technology. 81 (2012) 11–25.
[41] C. Guo, C. Xie, J. Zhang, S. Wang, D. Zhao, Experimental Investigation of the Resistance Performance and Heave and Pitch Motions of Ice-Going Container Ship Under Pack Ice Conditions, China Ocean Eng. 32 (2018) 169–178. https://doi.org/10.1007/s13344-018-0018-9.
[42] J.-H. Kim, Y. Kim, H.-S. Kim, S.-Y. Jeong, Numerical simulation of ice impacts on ship hulls in broken ice fields, Ocean Engineering. 180 (2019) 162–174.
[43] R.C. Woolgar, D.B. Colbourne, Effects of hull–ice friction coefficient on predictions of pack ice forces for moored offshore vessels, Ocean Engineering. 37 (2010) 296–303.
[44] B. Ni, D. Han, S. Di, Y. Xue, On the development of ice-water-structure interaction, Journal of Hydrodynamics. 32 (2020) 629–652.
[45] L. Huang, J. Tuhkuri, B. Igrec, M. Li, D. Stagonas, A. Toffoli, P. Cardiff, G. Thomas, Ship resistance when operating in floating ice floes: A combined CFD&DEM approach, Marine Structures. 74 (2020) 102817.
[46] M. Islam, J. Mills, R. Gash, W. Pearson, A literature survey of broken ice-structure interaction modelling methods for ships and offshore platforms, Ocean Engineering. 221 (2021) 108527.
[47] E. Anderlini, G.G. Parker, G. Thomas, Control of a ROV carrying an object, Ocean Engineering. 165 (2018) 307–318.
[48] F.U. Rehman, L. Huang, E. Anderlini, G. Thomas, Hydrodynamic Modelling for a Transportation System of Two Unmanned Underwater Vehicles: Semi-Empirical, Numerical and Experimental Analyses, Journal of Marine Science and Engineering. 9 (2021) 500.
[49] Z. Li, J.W. Ringsberg, F. Rita, A voyage planning tool for ships sailing between Europe and Asia via the Arctic, Ships and Offshore Structures. 15 (2020) S10–S19.
[50] A. Alberello, M. Onorato, L. Bennetts, M. Vichi, C. Eayrs, K. MacHutchon, A. Toffoli, Brief communication: Pancake ice floe size distribution during the winter expansion of the Antarctic marginal ice zone, The Cryosphere. 13 (2019) 41–48.
[51] IACS, Requirements Concerning Polar Class, International Association of Classification Societies (IACS). (2016).
[52] A.-S. Milaković, F. Li, M. Marouf, S. Ehlers, A machine learning-based method for simulation of ship speed profile in a complex ice field, Ships and Offshore Structures. (2019) 1–7.
[53] B. Pena, L. Huang, F. Ahlgren, A Review on Applications of Machine Learning in Shipping Sustainability, in: SNAME Maritime Convention, The Society of Naval Architects and Marine Engineers, 2020.
[54] B. Pena, L. Huang, Wave-GAN: A deep learning approach for the prediction of nonlinear regular wave loads and run-up on a fixed cylinder, Coastal Engineering. (2021) 103902.

[55] ITTC, 1978 ITTC Performance Prediction Method, Recommended Procedures and Guidelines. (2008).
[56] ITTC, general guidance and introduction to ice model test, ITTC Report. (2017).
[57] Z. Li, C. Ryan, L. Huang, L. Ding, J.W. Ringsberg, G. Thomas, A comparison of two ship performance models against full-scale measurements on a cargo ship on the Northern Sea Route, Ships and Offshore Structures. (2021). https://doi.org/10.1080/17445302.2021.1926146.
[58] J.N. Calleya, Ship design decision support for a carbon dioxide constrained future, PhD Thesis, UCL (University College London), 2014.
[59] F. Tillig, J.W. Ringsberg, W. Mao, B. Ramne, A generic energy systems model for efficient ship design and operation, Proceedings of the Institution of Mechanical Engineers, Part M: Journal of Engineering for the Maritime Environment. 231 (2017) 649–666.
[60] F. Tillig, Simulation model of a ship's energy performance and transportation costs, PhD Thesis, Chalmers University of Technology, 2020.
[61] M. Juva, K. Riska, On the power requirement in the Finnish-Swedish ice class rules, Winter Navigation Research Board, Res. Rpt. 53 (2002).
[62] E. Fiedler, M. Martin, E. Blockley, D. Lea, N. Fournier, Optimisation of sea ice forecasting for ship navigation, SEDNA, 2019.
[63] M.S. Committee, POLARIS–proposed system for determining operational limitations in ice, International Association of Classification Societies (IACS), 2014.
[64] Z. Li, J.W. Ringsberg, L. Ding, F. Rita, N. Fournier, J. Mendes, Safe and Fuel-Efficient Voyage Planning for the Northeast Passage by Combining Reliable Ship Performance, Weather and Ice Forecast Models, in: International Conference on Offshore Mechanics and Arctic Engineering, American Society of Mechanical Engineers, 2020: p. V007T07A005.